Abatan Abayomi (Orcid ID: 0000-0003-2330-3322)

Statistics of Multi-year Droughts from the Method for Object-Based Diagnostic Evaluation (MODE)

Abayomi A. Abatan[1,1,*], William J. Gutowski, Jr.[1], Caspar M. Ammann[2], Laurna Kaatz[3], Barbara G. Brown[2], Lawrence Buja[2], Randy Bullock[2], Tressa Fowler[2], Eric Gilleland[2] and John Halley Gotway[2]

[1]Department of Geological and Atmospheric Sciences, Iowa State University, Ames, Iowa USA
[2]Research Applications Laboratory, National Center for Atmospheric Research, Boulder, Colorado USA
[3]Denver Water, Denver, Colorado USA
[*]Department of Meteorology and Climate Science, Federal University of Technology, Akure, Nigeria

[1]Corresponding author address: Abayomi A. Abatan, 3134 Agronomy Hall, Department of Geological and Atmospheric Sciences, Iowa State University, Ames, Iowa 50011 USA.

E-mail address: abatanaa@iastate.edu yomiabatan69@gmail.com

Abstract

This study uses the Method for Object-based Diagnostic Evaluation (MODE) technique to examine and compare the statistics of drought attributes over the upper Colorado River basin (UCRB). The drought objects are based on the standardized precipitation index (SPI) and the standardized precipitation evapotranspiration index (SPEI) on a 36-month timescale (SPI36 and SPEI36, respectively). The drought indicators are calculated using monthly precipitation as well as minimum and maximum temperatures from the Precipitation-Elevation Regression on Independent Slopes Model datasets from 1948 to 2012. MODE uses paired object attributes such as centroid distance, orientation angle, area ratio, and intersection area and a combination of parameter thresholds to determine the number of objects identified and retained in the merging and matching process in the two fields. Using MODE run with convolution radius of 0 (no smoothing) and an area threshold of 4 grid points, this study computes and analyzes object statistics including centroid locations, areas and intensity percentiles. Results of the analysis show that SPI36 produces more drought objects than SPEI36. Although the spatial patterns are roughly similar leading up to almost similar statistics of object attributes, such as locations of the object centroids, the SPI36

produces higher percentile intensity of drought objects than does SPEI36, which is clearly obvious in the 90th percentile intensity of drought objects. The largest difference between SPEI36 and SPI36 occurs in the area of drought objects during the early 2000s when the region experienced multi-year drought resulting from increased warming of the atmosphere. This study demonstrates the use of MODE as a tool to evaluate and monitor drought event over the UCRB.

Keywords: MODE, SPEI, SPI, Drought objects, UCRB, Denver Water

1. Introduction

Droughts and pluvials are at the heart of many research studies because of their profound impact on water supplies (e.g., McCabe et al. 2004; Seager et al. 2008; Schubert et al. 2009; Cook et al. 2014a, 2014b). Recently, the potential changes in frequency, duration, magnitude and impacts of such events over the coming decades have gained attention (Meehl et al. 2000; Cook et al. 2015). Droughts and pluvials are opposing events that historically have had significant economic impact on various sectors including agriculture and water resources management. This makes them events of interest to a major water utility in our region of study, Denver Water. For example, the U.S. Department of the Interior Bureau of

Reclamation reported that "*Since 2000, the Colorado River Basin has been experiencing a historic, extended drought that has impacted regional water supply and other resources, such as hydropower, recreation, and ecologic services*". Reservoir storage in Lake Mead and Lake Powell has declined since the beginning of this persistent drought. Recently, Burgman and Jang (2015) estimated that drought-related agricultural loss in 2012 was worth tens of billions of U.S. dollars. Matthai (1969) reported that the 1965 flood on many streams in the South Platte River basin, resulting from three days of intense rains, caused damage worth US$508.2 million, with 75% of the losses recorded in the Denver metropolitan area. The 1976 catastrophic flash flood along the Big Thompson River left 139 dead, with an estimated property damage of US$35 million (Jarrett, 1990) while the historic Boulder flood of 9 – 15 September 2013 resulted in disaster emergencies being declared in 14 counties. These events can play an important role in depleting and polluting water systems and can lead to water shortages for both human consumption and agricultural purposes. Because of the potential impacts on ecosystems, humans, and animals, there is a great need for further understanding of the spatial characteristics of these extreme events.

Drought is complex in nature and it can be defined in different ways: agricultural, hydrological, meteorological, and socioeconomic (American Meteorological Society 1997; Dracup et al. 1980; Trenberth et al. 2007). The complexity of this extreme has resulted in its monitoring and characterization using different indices. This study builds on our previous work (Abatan et al. 2017) that used the standardized precipitation index (SPI; McKee et al.

1993; Guttman, 1998) and standardized precipitation evapotranspiration index (SPEI; Vicente-Serrano et al. 2010) to examine extended droughts and their associated physical processes for a multi-decadal period (36-month) in the upper Colorado River basin (UCRB). We use the SPI and SPEI because of their simplicity, widespread application, and endorsement by the World Meteorological Organization (WMO, 2006) and the research community as an important tool to monitor drought at different time scales and locations.

Previous studies on drought indices have typically relied on traditional verification metrics based on contingency tables and/or various forms of subjective visual evaluations. Often, these techniques can be misleading (Ahijevych et al. 2009), and they may not provide much information that is of interest to users (Davis et al. 2006a). The inherent limitations associated with traditional approaches have led to the development of novel, new spatial verification techniques, including various object-based methods (Ahijevych et al. 2009; Brown et al. 2011; Gilleland et al. 2009). Object-based techniques have obvious direct application to the study of drought areas; these methods include the Contiguous Rain Area approach (CRA; Ebert and McBride, 2000; Ebert and Gallus 2009), the Method for Object-based Diagnostic Evaluation (MODE; Davis et al. 2006a, 2006b, 2009), and the Structure-Amplitude Location approach (SAL; Wernli et al. 2008), amongst others. The SAL approach provides information about three specific characteristics of objects but has limited ability to directly compare sets of objects (Gilleland et al. 2009). The CRA approach estimates the magnitude of forecast error associated with forecast displacements, as well as biases in

overall intensity, and thus provides guidance regarding the amount of error that is not explained by these factors (denoted pattern error in the CRA formulation). One limitation of the CRA is that objects are matched only when they are contiguous (Gallus 2010). In contrast, the MODE approach does not require matched objects to be contiguous and is able to measure and compare a wide variety of object attributes (e.g., area, location, size, shape). This method makes it possible to evaluate characteristics of matched and unmatched objects in observed and model fields that would not be considered by the CRA (Davis et al. 2006a). Moreover, MODE is highly configurable and can be set up to meet the specific interests of individual users for specific applications (Bullock et al. 2016).

MODE was specifically developed for verification of gridded forecasts (e.g., from numerical weather prediction systems) compared to gridded observations. The method has largely been used to verify the forecasts of rainfall fields (e.g., Davis et al. 2006a, 2006b; Ahijevych et al. 2009; Davis et al. 2009; Gallus, 2010), which are difficult to evaluate due to the "double-penalty" issue in which displaced forecast fields are penalized as both false alarms and misses. Also, MODE has been applied to other meteorological variables, such as vector wind fields (Fowler and Bullock 2010). Mittermaier and Bullock (2013) used MODE and the time-domain version of MODE (which adds time as a third dimension) to explore the spatial and temporal characteristics of total cloud cover over the United Kingdom. However, until now, the application of object-based methods to climatological applications, such as drought evaluation have remained largely unexplored.

Here, we apply MODE to a climatological study of drought. We perform this exploration by comparing attributes of drought objects defined using the SPEI and SPI. We apply MODE to examine the spatial structure of spatially extensive droughts treated as objects. For this study, the drought objects are produced by SPEI and SPI at a 36-month timescale over UCRB. We focus on object attributes such as the location of object centroids, object areas, and intensity percentiles.

2 Study area, data and methods

2.1. The study area

As the name implies, UCRB is the upper division of the Colorado River in the American Southwest. The basin occupies an expanse of about 284,380 km^2. The flow from the UCRB, which is highly regulated by several compacts, serves the water requirements of the five basin states: northern Arizona, Colorado, New Mexico, Utah, and Wyoming (Figure 1). Diverse topographic features with the Wasatch Mountains in the west and the Rocky Mountains in the east characterize the basin. The relief ranges from 3,636 m (highest peak of the Wasatch; Mount Nebo) to 4,400 m (highest peak of the Rocky Mountains; Mount Elbert) above sea level. The complex topographic features result in the region experiencing difference climatic conditions. While the west is characterized by the maritime climatic conditions, the interior is characterized by continental climatic conditions. The region is semiarid in nature and the climate regimes over the basin that occur in the cold (October-

March) and warm seasons (April-September) is highly variable. The annual average temperature ranged from 5.1 to 7.9 °C, and the mean annual precipitation ranged from 510 to 1,060 mm. A large portion of the UCRB's accessible water comes from snowmelt during spring and heavy rainfall during summer (Christensen et al., 2004; Christensen and Lettenmaier, 2007). The precipitation events come mainly from frontal storms from the Pacific Ocean and convective storms whose moisture comes from the Gulf of Mexico or the Gulf of California (Barry, 1992).

2.2 Data

We use the monthly mean maximum and minimum temperatures and precipitation datasets from the Precipitation-Elevation Regression on Independent Slopes Model (PRISM; Daly et al. 1994, 2008) to derive the drought indices. We use PRISM as opposed to, say, station data because it provides observation-based data on a regular grid and it attempts to account for elevation effects that could be important in a mountainous region like the UCRB. The gridded datasets are available on a 4 km × 4 km spatial resolution from 1895–2012. However, we analyze data for the period 1948–2012 for consistency with our earlier study (Abatan et al., 2017). The analysis focuses on 36-month periods ending in December. For example, using a 36-month running window, the data for December 1950 is aggregated from the mean from January 1948 to December 1950. Similarly, data for December 1951 come from the mean from January 1949 to December 1951, etc. The focus on the 36-month

timescale was chosen to properly address the climate information needs of the Denver Water resources managers; in particular, the information necessary for planning water management, both for maintaining supply and adequate operating revenue.

2.3 Indices

Since there is no single method of assessing and describing drought severity that is suitable for all circumstances and users (Lloyd-Hughes, 2014), this study relies on the analyses of 36-month timescale SPEI and SPI to examine drought episodes over UCRB. The use of this timescale arises because Denver Water managers are especially interested in 36-month droughts for regional water resources planning and management.

The SPI is a multiscalar index developed for use in Colorado by McKee et al. 1993 to monitor drought and wet spells. The SPI algorithm, based solely on precipitation, permits expression of drought and wet spells in terms of precipitation deficits, percent of normal and probability distribution. The SPI is advantageous as it is simple to calculate and can be used effectively in all seasons of the year because of its avoidance of a dependence on soil moisture. This makes the index important for characterizing drought (wet spells) conditions for different applications. The multiscalar and standardization properties of SPI offers robust application of the index across different geographical regions at different timescales. At shorter timescales (e.g., 3 and 6 months) SPI can be used to indicate agricultural and meteorological drought, while at longer timescale it is useful for hydrological drought.

But there are also shortcomings to SPI. Since SPI is based on precipitation data alone, it fails to account for the influence of evaporation and transpiration on the climatic water balance. Hayes et al. (1999) indicated that application of SPI at shorter timescales (1, 2, or 3 months) in regions with normally low seasonal precipitation totals can be misleading because SPI gives a similar result to the percent of normal representation of precipitation. Despite these limitations, SPI has gained widespread acceptance and use because of its versatile and simple nature. Detailed expositions of the SPI methodology and applications can be found in studies such as McKee et al. (1993), Guttman, (1998), Lloyd-Hughes and Saunders (2002).

Vicente-Serrano et al. (2010) proposed the SPEI as an extension to the SPI as a more sensitive tool for drought evaluation for a changing climate. It is a modification of the SPI that incorporates potential evapotranspiration in its algorithm using the Hargreaves formula (Hargreaves and Samani, 1985), thus allowing for a more refined evaluation of the surface water balance. As a result, SPEI combines the advantages of being multiscalar (like the SPI) and accounting for the contribution of temperature to water balance (Chen et al. 2013). The SPEI is obtained by fitting a log-logistic Pearson III distribution to the climatic water balance. Details appear in Vicente-Serrano et al. (2010), Beguería et al. (2014), and Yu et al. (2014).

We calculate the 36-month SPEI and SPI (hereafter SPEI36 and SPI36) based on the PRISM monthly rainfall and temperature (minimum and maximum) values at each grid point over the UCRB using the SPEI library (Beguaría and Vicente-Serrano, 2013) developed for

the R software suite (R Development Core Team, 2012). As stated earlier, we define the drought indices at 36-month starting from January and ending in December of the third year for annual increments over the period 1950–2012 and we focus further analysis only on the periods ending in December.

2.4 MODE

MODE is an object-based technique that represents a class of spatial verification methods. The MODE technique was developed independently for weather forecast verification purposes by Davies et al. (2006a, 2006b), but follows the same overall paradigm as earlier work in the field of image analysis proposed by Chen and Wang (2002). The objective is to identify localized and episodic features of interest in 2-dimensional scalar fields and compare features in the two fields (generally a forecast and an observed field) to identify which features best correspond to each other (Davies et al. 2009). The MODE process involves object identification based on specified thresholds, object attributes measurement, objects merging, objects matching, and comparison of object attributes between the two fields. MODE is inherently flexible. It allows users to determine how merging and matching of objects in two fields are implemented. In addition, as in this study, MODE can be adapted to better meet the specific verification needs of the user (Davies et al. 2006a). This implies that the user can specify parameters of interest (such as centroid location, shape {orientation angle and aspect ratio}, intensity, area) and compute their

statistics (such as standard deviation, median of intensity percentiles, maximum of median interest (MMI)) for individual objects in either field, and for the identified (matched) pairs of objects between the two fields. Therefore, MODE offers users a flexible way to learn about specified characteristics in individual datasets, but also immediately about commonalities (hits) and differences (misses) between, traditionally, a forecast and observations. Of course, we can use MODE to characterize any one or more fields, none has to be an observation, and both can be different observational datasets without involving forecast or other model output. In essence, MODE may be used to compare any two fields (field1 and field2). In this study, field1 is SPEI36, while field2 is SPI36. As MODE normally operates on two input datasets, we use SPEI36 and SPI36, respectively as input fields.

MODE uses two basic steps to identify objects in meteorological fields. First, the raw data is convolved. This is basically a smoothing process using a convolution radius to remove unnecessary local scale variability. Secondly, the convolved data field is masked by applying a threshold (T) on the intensity of the fields, returning a binary matrix of zeroes, where the threshold was not surpassed, and non-zeroes (ones), where the selection criteria (threshold) were fulfilled. This can be done for multiple criteria, and where all of them pass their corresponding thresholds, these locations are then further analyzed, while any other information in cells that don't fulfill the thresholds are eliminated.

To identify coherent objects, and to compare objects between the fields, a step called "merging and matching" is performed (for details see Davies et al. 2006a, 2006b, and

Bullock et al. 2016). MODE uses a fuzzy logic algorithm (Yager et al. 1987) to merge the retained information of the masked convolution fields into contiguous areas (objects). This is done individually in both forecast and observed fields. Using an iterative process, the "matching" step then attempts to identify corresponding objects between forecast and observed fields. The fuzzy logic algorithm considers many attributes of the objects to calculate a metric known as the total interest function that ultimately determines which objects are to be merged and matched. The attributes of each object pair used as input in the fuzzy logic engine to calculate the total interest are centroid distance separation, orientation angle difference, intersection area, and area ratio. Given two objects, the area ratio is calculated by dividing the area of the smaller object by the area of the larger object, while the intersection area is the fraction of the overlap area divided by the average of the areas of the two objects. Other attributes of interest include union area and symmetric difference. The union area is the total area that is in either one or both of the two objects, and the symmetric difference is the area inside at least one object, but not both. Further details on the object pair attributes and the computation of the total interest appear in Davies et al. (2009) and Johnson and Wang (2012). For guiding the precise identification of a match between objects in the two fields, the total interest function is assigned a threshold value. MODE typically uses a total interest threshold value of 0.7. Pairs of objects in the two fields that exceeds this threshold value are considered a match. For all matches, the values in the masked convolution field are then replaced with the original values in order to retain the real

intensities (note, the convolution led to an artificial smoothing to reduce noise, but for locations identified as part of objects, the true intensities are needed). All statistics are then calculated for each pair of matched objects as well as for each single objects in the separate fields.

MODE is run once all the necessary input and parameter thresholds are set. The summary statistics generated are written separately for each 36-month into the MODE output database, where they are available for inspection, analysis, and synthesis. The output files contain information for all of the attributes for individual drought objects (simple and merged cluster) and matched drought objects (simple pairs and cluster pairs). Detailed information can be found in the MET_Users_Guide[2]. Among the information in the output file for individual objects is the percentile of intensities (e.g., 10th, 50th, and 90th) inside the object, the centroid locations of the object, and the area of the object. However, for matched objects, MODE output such statistics as critical success index, total interest, and intersection area. Other statistics such as bias can be calculated for the matched objects. For the climatology analysis in section 3.3, we extract the median value of the attributes of interest for each drought index separately and for each year to form a time series (an example is shown in Table 3 for 1960). Then we compare the temporal evolution of the median of the attributes of drought objects from SPEI36 and SPI36 using a box-whisker plot. Prior to the analysis in this study, we perform a normality test on the time series of the attributes to assess if the data

[2] https://dtcenter.org/met/users/docs/overview.php

series are normally distributed (see Appendix A1–A2). For the time series that are normally distributed, we use the Welch Student's *t* test to assess the significant of the difference of two means for SPEI36 and SPI36 series, while we use Kolmogorov-Smirnov test statistics for the non-normally distributed series. Because the area of drought objects vary spatially, we take the logarithm of the area time series for clarity of analysis. Further, we use the paired *t* test to assess the statistical significance of the difference in distributions of the median of attributes of merged cluster drought objects between SPEI36 and SPI36.

2.5 Parameter threshold

Objects are identified in the two fields and statistics of attributes of the objects are calculated and compared. Next, we take average of the statistics of object attributes in order to obtain the climatological characteristics of SPEI36 and SPI36 drought and pluvial objects. Thus, comparisons are at the climatological level.

As previously stated, MODE determines the number of objects retained in the merging and matching process by a combination of the convolution radius, area threshold, and the intensity threshold. This implies that variations in these parameters can impact the number of objects identified. It is worth noting that Davies et al. (2006a) suggested a minimum convolution radius of four grid lengths. We performed a sensitivity analysis to examine the influence of different parameter choices on the number of objects. For the drought analysis (intensity threshold <= –1.0), four cases were examined to compare the number of resulting

objects. We use: 1) convolution radius equal 0 (no smoothing) and an area threshold of 4 (hereafter; R0A4D), meaning that only contiguous regions of at least 4 connected grid-cells would make up objects; 2) convolution radius equal 4 and area threshold of 4 (R4A4D); 3) convolution radius equal 0 and area threshold of 6 (R0A6D); and 4) convolution radius equal 4 and area threshold of 6 (R4A6D). We repeated the same case samples for pluvial (intensity threshold of +1.0), leading to 1) R0A4P; 2) R4A4P; 3) R0A6P and 4) R4A6P. For the analysis presented in the next section, we focus on some of the attributes relevant for the study domain, such as centroids location, area and intensity percentiles. Lastly, we compute and compare the statistics of these attributes for the SPEI36 and SPI36.

3. Results and discussion

3.1 Sensitivity to threshold selection

In order to explore the sensitivity of the results to the retained number of objects and to selected parameter threshold, we applied MODE analysis to PRISM-derived SPI and SPEI using different combinations of area threshold and convolution radius. Figure 2 shows the temporal evolution of the number of drought objects identified for different combinations of parameter choices. For clarity of text, Table 1 gives an overview of the number of objects for each index and for each parameter threshold. It can be seen that the number of objects is very sensitive to the combination of parameter choices. In particular, it appears that the number of

objects depends more strongly on the value of convolution radius, and less on the area threshold. Although R0A4 and R0A6 show similar patterns (Figs. 2a, b), the number of objects produced by both SPEI36 and SPI36 for the R0A4 combination is higher than in R0A6 (Table 1).

A similar temporal pattern (Figs. 2c, d) and approximately an equal number of objects (Table 1) is found for the comparison between R4A4 and R4A6 for drought events. However, there is a large disparity in the number of objects between R0A4 and R4A4, and also between R0A6 and R4A6. The SPEI (SPI) R4A4 objects is about 42% (36%) of SPEI (SPI) R0A4 objects, while SPEI (SPI) R0A6 drought objects is slightly more than twice SPEI (SPI) R4A6 objects. The contribution of convolution radius to the number of objects is noteworthy; while the area threshold has little influence, the convolution radius is dominant in determining the number of retained objects. Comparison of the number of retained objects due to a combination involving R0 and R4 indicates that the higher number of objects in this study benefits from the case with no convolution radius (R0). Because we use indices based on monthly average data that are aggregated over a further 36-month timescale, it is reasonable to suggest that the resulting fields are already very smooth, and further smoothing of the indices using a convolution radius of four grid lengths as suggested by Davies et al. (2006a) is not necessary for this study, and in fact, convolution might further water down the signal.

The figures give evidence on the selection of reasonable values of area threshold for defining objects. So, given the above results, we conclude that a combination of convolution radius of zero (R0) and area threshold of four grid lengths (A4) is ideal for producing sufficient number of objects to allow statistical analyses, while avoiding objects with only one or two grid points, which might represent a structure too small to resolve. Having a good number of objects will also permit an adequate statistical analysis of the object attributes. Hence, for the remaining analysis in this study, we compare the statistics of SPEI36 and SPI36 drought objects attributes using MODE run with R0A4 parameter selection.

3.2 Sample output of MODE objects and attributes

Figure 3 shows the results of the application of MODE to SPEI36 and SPI36 datasets for 1960. The spatial distribution of drought in SPEI36 and SPI36 is shown in Figs. 3a and 3b, while the merged cluster of single drought objects identified for SPEI36 and SPI36 is shown in Figs. 3c and 3d. The colored numbers in the figures indicate cluster pairs of objects that were matched between the two fields. While Table 2 presents the total interest values of the simple single drought objects between the two indices, Table 3 gives the information and statistics of merged cluster drought objects identified by the two drought indices (Fig. 3). From Table 2, there are 7 simple single drought objects in SPEI36 and 10 simple single drought objects in SPI36 fields.

The aggregated total interest values (Table 2) indicate a good match between the simple single drought objects depicted by the two drought indices (not shown). The total interest values for the matched objects are considerably higher than the 0.7 thresholds; the values range from 0.7046 to 1.00. In particular, there is a perfect match in SPEI36–SPI36 simple drought object pairs (1, 1), (2, 2), and (6, 7), with a total interest of 1.00. The statistics of some of the attributes of these objects reflect this good match (Table 3). Using the 0.7 total interest threshold, we observe a match between SPEI36 object 4 and SPI36 objects 4 and 5. Because there is a double match with SPEI36 object 4, SPI36 objects 4 and 5 are considered as a cluster. Similarly, there is a match between SPI36 object 7 and SPEI36 objects 5 and 6. The result of a double match with SPI36 object 7 yields a cluster of SPEI36 objects 5 and 6. Hence, the merging of objects within each field and the corresponding matching of simple object pairs between the two fields result in a total of 6 matched (merged cluster) objects between SPEI36 and SPI36 fields (Figs. 3c and 3d).

The total object area in SPEI36 is 14024 grid-points, while it is 12557 grid-points in SPI36 (Table 3). The difference in area between the matched object pairs is about 10%, or 1467 grid-points. Also, differences between the centroids distance are small, indicating that both drought indicators produce objects at about the same location. For instance, the centroid distance for cluster pairs object 2 is 0.37, while it is 4.5 for cluster pairs object 6 (Fig. 3). Consistent with the objects area and centroids, the median of drought intensity within the objects vary slightly from one object to another. For example, the median of the 50th

percentile intensity of drought objects ranges from –1.05 to –1.59 in SPEI36, while it ranges from –1.05 to –1.58 in SPI36.

Overall, the sample result presented here indicates that both SPEI36 and SPI36 produced drought objects over UCRB, although there is a slight difference in magnitude, location, and areal extent. The climatology of individual objects, in which this sample is a part, will be discussed in section 3.3, while the statistics of matched objects (cluster pairs) will be addressed in section 3.4.

3.3 Results of individual drought objects

3.3.1 Statistics of simple single drought objects

This section examines and compares the distributions of the median values of various object attributes (e.g., intensity {e.g., 10th, 50th and 90th percentiles}, centroid location {latitude and longitude}, and area) for all simple single drought objects from SPI36 and SPEI36.

Table 4 shows the summary of the mean values of the median of the 10th, 50th, and 90th percentiles intensity, centroid location, and area attributes of SPI36 and SPEI36 drought objects. Although the median of the percentile intensity attributes from SPI36 compared well with that from SPEI36, there are still slight differences. The SPI36 has drought intensities that are slightly higher than that of SPEI36 (Fig. 4). For the 10th percentile intensity attribute, the mean intensity for SPI36 is approximately the same with that of SPEI36 (Fig. 4a). The

difference in mean intensity between the two indices, calculated using the Kolmogorov-Smirnov two-sample test statistics for non-normal data (Appendix A1) at the 5% level, is not statistically significant (p-value = 0.37). For the 50th percentile intensity attribute (Fig. 4b), the mean drought intensity in SPEI36 is slightly lower than that of SPI36 (Table 4). Similarly, the difference in mean for the 50th percentile intensity attribute of the drought objects is not statistically significant (p-value = 0.08). The Kolmogorov-Smirnov test of significance for the difference between the two means indicates that the difference in mean of the 90th percentile intensity attribute of the drought objects from SPI36 and SPEI36 is not statistically significant at the 5% level as p-value equal 0.06.

The summary of the mean values of centroid locations (latitude and longitude) of drought object for SPI36 versus SPEI36 is shown in Table 4. For SPEI36, the median value of centroid latitude ranges from 36.0 to 42.5 °N, while for SPI36 it ranges from 36.4 to 41.9 °N. On average, the statistics of centroid latitude of drought objects show that the latitudes of drought objects retained by the two indicators are comparable, with approximately similar mean values. Based on the Student's *t* test, there is no significant difference between their means ($t = 0.09$, p-value = 0.93). As in the centroid latitude, the median of centroid longitude for SPEI36 ranges from 106.5 to 110.8 °W, while for SPI36 it ranges from 106.5 to 111.8 °W. Although both indicators locate the drought object at about the same longitude, objects in SPI36 are displaced slightly further west than in SPEI36. The test of significance for the difference of two means indicate non-significant difference between the means of the

centroid longitude of drought objects from the two indices; t = –0.07, p-value = 0.94. In general, the statistics of centroid locations of drought objects in SPEI36 and SPI36 are similar.

As with the number of objects identified by the two indices, the size of drought area can vary; leading to different median and mean values among two fields. So, given the fact that the area of drought objects vary in size and structure, the idea here is to examine the distributions of the median and mean values and then assess which of these statistics is suitable to represent the area attribute of drought objects. For 2007 drought, SPEI36 identified 2 simple drought objects with areal extent given as {15, 1046}, leading to mean and median having the same value (530.5 grids), respectively. On the other hand, SPI36 has 4 simple drought objects. The areal extent in rank order gives {6, 14, 17, 461}, leading to mean value of 124.5 grids and median value of 15.5 grids. Above results indicate the impact of the number of objects on both statistics. Overall, the Kolmogorov-Smirnov test indicates that the difference in mean of the mean value of area attribute of the drought objects between SPI36 and SPEI36 is not statistically significant at the 5% level as p-value equal 0.2921. Similarly, there is no significant difference in mean of the median value of area attribute of the drought objects between SPI36 and SPEI36 (p-value = 0.4055). These results suggest that users can and should apply the statistics that is appropriate to their need.

3.3.1.1 Composite statistics of simple single drought objects

This section summarizes the statistics of distributions discussed earlier, using concise box-whisker plots. The box-whisker plots offer a simple yet visually striking comparison of the drought attribute statistics. For the climatology of each of the object attributes in section 3.3.1, we extract a full range of statistics, such as the 5th percentile, first-quantile (25th), median, third-quantile (75th), 95th, and mean.

Figure 4 shows the statistics of 10th, 50th, and 90th percentile intensity attributes of drought intensity within objects for SPEI36 and SPI36 for the period of 1950–2012. The median of drought intensity for SPEI36 and SPI36 are slightly different from each other. Also, the spread in SPI36 is slightly wider than in SPEI36. Once more, this is likely the result of the number of drought objects identified (Fig. 2a). The median value of the 10th percentile intensity attribute is –1.02 and –1.03 for SPEI36 and SPI36, respectively. The 50th percentile intensity attribute shows that median value in SPEI36 is about 2% lower than that of SPI36. The median values are –1.08 and –1.10 for SPEI36 and SPI36, respectively. In contrast to the 10th and 50th percentile intensity attributes, the 90th percentile intensity attribute has large median difference. The median values for SPEI36 and SPI36 drought objects are –1.17 and –1.22, respectively. This indicates that SPI36 has severe drought intensities within the objects than SPEI36, even though mean values are nearly the same.

Figure 5 shows the distribution of statistics of the median of centroid location attribute for SPEI36 and SPI36. For the centroid latitude of drought objects, although the statistics are

quite close, the distribution of the median statistics is slightly more spread out in SPI36 than in SPEI36 (Fig. 5a). However, Fig. 5b shows that centroid longitude of drought objects in SPI36 is located slightly west of the location in SPEI36, with the spread in location also greater than that of SPEI36.

Figure 6 shows the statistics of area attribute of drought objects from SPEI36 and SPI36. Consistent with the spread in the percentile intensity attribute, the spread in drought area is slightly wider in SPI36 than in SPEI36 further showing that the area of some of the drought objects in SPI36 is larger than in SPEI36. Although the median value of the distributions is the same, there are differences in other statistics. For example, both indices skewed to the right, but the tails are slightly different. Similarly the temporal mean in SPI36 is higher than in SPEI36 (Table 4).

3.3.2 Statistics of merged cluster drought objects

Further, we analyze the relationship between SPEI36 and SPI36 for merged cluster drought objects. We assess the statistical significance of the difference in distributions using the paired *t* test at the 5% level. As in the previous section, we present results only for intensity, centroids, and area attributes. As shown in Figure 7, there is a linear relationship between the two indices, although some scatter exists between the indices. For the 10% quantile attribute of drought intensity, the difference in intensity between the two indices during the period of study is very small, although SPI36 has higher magnitude at about 67%

of times. These values range between –0.03 and 0.15, with the exception of 2002 and 2003 where the magnitude of the difference are –0.27 and –0.19, respectively. With this distribution, the paired *t* test indicates that there is no significant difference (p-value = 0.9394) in the 10% quantile attribute of drought intensity from the two drought indices. The distribution of the difference in the 50% quantile attribute of drought intensity between SPEI36 and SPI36 shows that the values vary between –0.18 and 0.41, with SPI36 having higher drought magnitude than SPEI36 at about 75% of times. The analysis is supported with a paired *t* test statistic, where result shows that the difference is considered to be statistically significant (p-value = 0.0004). A similar result is shown for the 90% quantiles, where SPI36 exhibits higher drought intensity (85%) than in SPEI36 (14%). However, it is noted that SPEI36 clearly identify higher drought intensity during the 2000s. The difference in drought intensity identified by the two indices ranges between –0.17 and 0.75. The difference in the 90th percentile intensity attribute of drought objects between SPEI36 and SPI36 is statistically significant (p-value = 0.0001). Figure 8 shows the relationship between the drought indicators for the centroid locations of the merged cluster drought objects. A linear relationship exist between the SPEI and SPI centroid latitude (Fig. 8a), suggesting that both indices produce matched drought objects over UCRB at almost the same location. The result of the paired *t* test indicates that there is no statistically significant difference (p-value = 0.6969) between the distributions of the SPEI and SPI centroid latitude. Similarly, we observe a nearly perfect relationship between SPEI36 and SPI36 for MODE centroid

longitude (Fig. 8b). As indicated by the paired *t* test statistic, the difference in the distributions of centroid longitude of merged cluster drought objects between the SPEI and SPI is not statistically significant (p-value = 0.8521). Figure 9 shows the scatter plots of the median and mean of area of merged cluster drought objects over UCRB. Few outliers are observed in the distributions of both the median and mean values of area of merged drought objects. Also, differences in the spatial patterns of the area of drought objects are evidence, as the scatter points deviates from the diagonal lines. The paired *t* test indicates that there is a statistically significant difference between the distributions of the SPEI36 and SPI36 area of drought objects. The p-value for median and mean values of area of merged cluster drought objects are 0.006 and 0.003, respectively.

3.4 Results of matched drought objects

3.4.1 Statistics of cluster pairs of drought objects

Apart from the statistics of individual object attributes previously analyzed, MODE output files also provide information on the commonalities of drought objects from the two indices that can be explored. Among such information are the critical success index (CSI), the area and intensity biases. The object-based CSI is a measure of the frequency of matched objects. It is defined as the ratio of hits to the sum of hits, misses, and false alarms. In this study, an object is defined and counted as a miss when SPI-produced drought objects have no match in SPEI, while a false alarm is counted when SPEI objects have no match in the SPI.

This definition is analogous to that defined for forecast and observed systems (Davis et al. 2006a, 2006b).

Figure 10 shows the evolution of CSI over UCRB for the period 1950–2012. The gaps in the temporal pattern is a result of no drought objects during the period (Fig. 2a). The CSI is characterized by substantial interannual variability with higher values that indicate similarities between the spatial pattern of SPEI36 and SPI36 drought objects. Lower CSI values (< 1 standard deviation; 1Ã= 0.28) occur at about 27% of times, again confirming the similarity between the drought objects identified by the two indices. Further to the CSI, biases in the drought object attributes are examined. The area bias for all matched cluster pairs of drought object normalized by the average of all matched SPI36 areas for a given year is given as;

$$B^t_{area} = \frac{\sum_i \left[A^t_{spei,i} - A^t_{spi,i}\right]}{\sum_i A^t_{spi}} \quad (1)$$

Analogously, the intensity bias is given as;

$$B^t_{intensity} = \frac{\sum_i \left[I^t_{spei,i} - I^t_{spi,i}\right]}{\sum_i I^t_{spi}} \quad (2)$$

where *B* refers to bias and the superscript *t* refers to the year when there is drought object.

Figure 11 shows the temporal evolution of area and percentile intensity biases for cluster pairs of drought objects. As shown in Fig. 11a, the area bias is very small confirming that both SPEI36 and SPI36 have roughly similar matched object sizes; supporting the CSI result.

However, there are periods when the drought object area in SPEI36 is wider than in SPI36, and vice-versa. With this, the area bias lies between ± 1Ã at about 86% (43 of 50) of times. The area of drought objects identified by SPEI36 is wider than that of the SPI36 only 4 times (bias > 1Ã), while the area of drought objects identified by SPI36 is wider than that of the SPEI36 only 3 times (bias < 1Ã). The bias in 10th and 90th percentile intensities within the cluster pairs of drought object areas is shown in Fig. 11b. The bias in 10th percentile intensity is small with values lying between ± 1Ã at about 70% of the period. SPI36 has higher intensity values than SPEI36 at about 22% (11) of the period (bias < 1Ã). Unlike the 10th percentile intensity, the negative bias in 90th percentile intensity of drought object is obvious. This shows that SPI36 has more severe droughts than those identified by SPEI36 during the period of study. The earlier period of the study from 1950 to 1980 is characterized by strong negative bias, while some of the later period from 1981 to 2012 is dominated by periods with no drought objects. This pattern is consistent with Figures 3d, 3e, and 5b of Abatan et al. (2017), although with differences in extreme magnitudes.

4. Conclusions

We use the MODE technique to examine and compare the statistics of attributes of drought objects from the SPEI and SPI at 36-month timescale UCRB. The two drought indicators are calculated using the monthly climate variables from PRISM datasets from

1948 to 2012. MODE identifies several parameters of interest, but, in particular, we focus on object attributes such as centroid location, area and intensity percentiles. To the best of authors' knowledge, MODE has been widely used to obtain statistics of attributes of the objects of wet extremes at weather timescales, but it has not been used to examine drought characteristics. Because of this, we perform a sensitivity test to determine the best combination of parameter thresholds suitable for the number of objects identified and retained in the merging and matching process. We observe that a combination of convolution radius equal 0 (no smoothing) and an area threshold of 4 grid points is well suited for this study, contrary to a minimum of convolution radius of four grid lengths suggested by Davies et al. (2006a) for precipitation evaluation. This study provides an important first-hand information in using MODE to examine multi-year drought conditions over UCRB.

The distribution of the median of the percentile intensity of drought objects from SPI36 is similar to that from SPEI36, although slight differences exist. We find that SPI36 has severe drought intensities, but, the Kolmogorov-Smirnov test statistics for the difference of two means indicates that the difference in means is not statistically significant. However, using the paired *t* test for the distributions of the merged cluster drought objects, the results show that there is a statistically significant difference between the two drought indices. Despite the differences in intensity, the climatology results show that both indices place the centroids (latitude and longitude) of the drought objects at about the same location.

The area of drought objects is characterized by substantial variability in size and number. From the analysis of the individual objects, we find that SPI36 has more and larger drought objects than does SPEI36. However, MODE clearly identifies the 2000s multi-year droughts over the study domain that peaked in 2002 in SPEI36, consistent with the previous study by Abatan et al. (2017). This further highlights the importance of MODE utility in drought analyses. Being the first time that MODE is being used in drought analysis, we point out that object based verification methods, including MODE can complements existing methods. In other words, users, such as Water resource managers can gain a greater understanding for the features of interest, in this case, hydrological drought, by looking at multiple metrics.

In order to examine further the similarities/differences between the two drought indicators, we analyze the object-based CSI and area and intensity biases of the matched drought objects. The higher value of CSI during the period of study is suggestive of a similarity between the area of matched drought objects identify by SPEI36 and SPI36. The negative bias in the 90th percentile intensity of drought objects further attests that some of the matched drought objects in SPI36 have more severe droughts that in SPEI36.

In conclusion, at the timescale considered in this study, SPI produces higher percentile intensity of drought objects, which is clearly obvious in the 90th percentile intensity of drought objects. Although both indices produced drought objects at about the same location over UCRB, the large difference between SPEI36 and SPI36 occurred in the area of drought objects during the recent period when UCRB experience drought conditions, which previous

studies have linked to ongoing global warming. This indicated that drought indices that include the effects of temperature are increasingly important for drought evaluation and monitoring over UCRB.

Acknowledgements

We acknowledged the comments and contributions of the reviewers. This work is supported by the National Science Foundation through Earth System Modeling (EaSM) Grant AGS-1243030. We acknowledge high-performance computing support from Yellowstone (ark:/85065/d7wd3xhc) provided by NCAR's Computational and Information System Laboratory. NCAR is supported by the National Science Foundation, and managed by the University Corporation for Atmospheric Research. We also thank the management of the Federal University of Technology, Akure, Nigeria for granting study leave to the first author. To God be all the glory.

References

Abatan AA, Gutowski WJ Jr., Ammann CM, Kaatz L, Brown BG, Buja L, Bullock R, Fowler T, Gilleland E, Gotway JH. 2017. Multi-year droughts and pluvials over Upper Colorado River basin and associated circulations. *J. Hydrometeor.,* **18,** 799–818, doi: 10.1175/JHM-D-16-0125.1.

Ahijevych D, Gilleland E, Brown BG, Ebert EE. 2009. Application of spatial verification methods to idealized and NWP-gridded precipitation forecasts. *Wea. Forecasting* **24:** 1485–1497.

American Meteorological Society. 1997. Meteorological drought—Policy statement. *Bull. Amer. Meteor. Soc.* **78:** 847–849.

Barry, R. G., 1992: Mountain weather and climate. Routledge, New York, 402 pp.

Beguería S, Vicente-Serrano SM. 2013. Calculation of the Standardised Precipitation-Evapotranspiration Index (SPEI). Available from: http://cran.r-project.org/web/packages /SPEI/SPEI.pdf [9 June 2015]

Beguería S, Vicente-Serrano SM, Fergus F, Latorre B. 2014. Standardized precipitation evapotranspiration index (SPEI) revisited: parameter fitting, evapotranspiration models, tools, datasets and drought monitoring. *Int. J. Climatol*. **34:** 3001–3023.

Brown BG, Gilleland E, Ebert E. 2011. Forecasts of spatial fields, Chapter 6, pp. 95–117, In: *Forecast Verification: A Practitioner's Guide in Atmospheric Science*, I. T. Jolliffe and D. B. Stephenson, Eds., John Wiley & Sons, Ltd, 274 pp.

Bullock RG, Brown BG, Fowler TL. 2016. *Method for Object-Based Diagnostic Evaluation*. NCAR Technical Note NCAR/TN-532+STR, 84 pp, doi:10.5065/D61V5CBS. Available from http://opensky.library.ucar.edu/search/?ky=technotes.

Burgman RJ, Jang Y. 2015. Simulated U.S. drought response to interannual and decadal Pacific SST variability. *J. Climate* **15:** 4688–4705.

Chen Y, Wang JZ. 2002. A region-based fuzzy feature matching approach to content-based image retrieval. *IEEE Pattern Anal. Mach. Intell*. **24:** 1252–1267.

Chen T, van der Werf GR, de Jeu RAM, Wang G, Dolman AJ. 2013. A global analysis of the impact of drought on net primary productivity. *Hydrol. Earth Syst. Sci*. **17:** 3885–3894.

Christensen NS, Lettenmaier DP. 2007. A multimodel ensemble approach to assessment of climate change impacts on the hydrology and water resources of the Colorado River Basin. *Hydrol. and Earth System Sci.* **11:** 1417–1435.

Christensen NS, Woods AW, Voisin N, Lettenmaier DP, Palmer RN. 2004. The effects of climate change on the hydrology and water resources of the Colorado River Basin. *Climatic Change* **62:** 337–363.

Cook BI, Seager R, Smerdon JE. 2014a. The worst North American drought year of the last millennium: 1934. *Geophys. Res. Lett*. **41:** 7298–7305, doi: 10.1002/2014GL061661.

Cook BI, Smerdon JE, Seager R, Coats S. 2014b. Global warming and 21st century drying. *Clim. Dyn.* **43:** no. 9-10, 2607–2627, doi: 10.1007/s00382-014-2075-y.

Cook BI, Ault TR, Smerdon JE. 2015. Unprecedented 21st century drought risk in the American Southwest and central Plains. *Science Advance* **1:** 1–7.

Daly C, Halbleib M, Smith JI, Gibson WP, Doggett MK, Taylor GH, Curtis J, Pasteris PP. 2008. Physiographically-sensitive mapping of temperature and precipitation across the conterminous United States. *Int. J. Climatol*. **1:** 2031–2064.

Daly C, Neilson RP, Phillips DL. 1994. A statistical–topographic model for mapping climatological precipitation over mountainous terrain. *J. Appl. Meteor.* **33:** 140–158.

Davis C, Brown B, Bullock R. 2006a. Object-based verification of precipitation forecasts. Part I: Methods and application to mesoscale rain areas. *Mon. Wea. Rev*. **134:** 1772–1784.

Davis C, Brown B, Bullock R. 2006b: Object-based verification of precipitation forecasts. Part II: Application to convective rain systems. *Mon. Wea. Rev*. **134:** 1785–1795.

Davis CA, Brown BG, Bullock R, Halley-Gotway J. 2009. The Method for Object-based Diagnostic Evaluation (MODE) applied to numerical forecasts from the 2005 NSSL/SPC Spring Program. *Wea. Forecasting* **24:** 1252–1267.

Dracup JA, Lee KS, Paulson EG. 1980. On the statistical characteristics of drought events. *Water Resources Research* **16:** 289–296.

Ebert EE, Gallus WA. 2009. Toward better understanding of the Contiguous Rain Area (CRA) method. *Weather and Forecasting* **24:** 1401–1415.

Ebert EE, McBride JL. 2000. Verification of precipitation in weather systems: Determination of systematic errors. *J. Hydrol*. **239:** 179–202.

Fowler TL, Bullock R. 2010. Examination of Spatial Wind Features Associated with Ramping Events using MODE. First Conference on Weather, Climate, and the New Energy Economy. American Meteorological Society, Atlanta, January 16–20, 2010.

Gallus WA Jr. 2010. Application of Object-based verification techniques to ensemble

precipitation forecasts. *Wea. Forecasting* **25:** 144–158.

Gilleland E, Ahijevych D, Brown BG, Casati B, Ebert EE. 2009. Intercomparison of spatial verification methods. *Wea. Forecasting* **24:** 1416 – 1430.

Guttman NB. 1998. Comparing the Palmer drought index and the standardized precipitation index. *J. Amer. Water Resources Assoc*. **34:** 113–121.

Hargreaves GL, Samani ZA. 1985. Reference crop evapotranspiration from temperature. *Appl. Eng. Agric.* **1:** 96–99.

Hayes MJ, Svoboda MD, Wilhite DA, Vanyarkho OV. 1999. Monitoring the 1996 drought using the Standardized Precipitation Index. *Bull. Amer. Meteor. Soc*. **80:** 429 – 438.

Jarrett RD. 1990. Paleohydrologic techniques used to define the spatial occurrence of floods. *Geomorphology* **3:** 181–195.

Johnson A, Wang X. 2012. Verification and calibration of neighborhood and object-based probabilistic precipitation forecasts from a multimodel convection-allowing ensemble. *Mon. Wea. Rev*. **140:** 3054–3077.

Kalnay E, and Coauthors. 1996. The NCEP/NCAR 40-Year Reanalysis Project. *Bull. Amer. Meteor. Soc*. **77:** 437–471.

Lloyd-Hudges B. 2014. The impracticality of a universal drought definition. *Theor. Appl. Climatol*. **117:** 607–611.

Lloyd-Hughes B, Saunders MA. 2002. A drought climatology for Europe. *Int. J. Climatol*. **22:** 1571–1592.

Matthai HF. 1969. Floods of 1965 in the United States: Floods of June 1965 in South Platte River basin, Colorado. U.S. Government printing office, Washington, D.C. 20402. Geological survey water-supply paper 1850-B. pp62.

Mittermaier MP, R Bullock. 2013. Using MODE to explore the spatial and temporal characteristics of cloud cover forecasts from high-resolution NWP models. *Meteor. Applications* **20:** 187–196.

McCabe GJ, Palecki MA Betancourt JL. 2004. Pacific and Atlantic Ocean influences on multidecadal drought frequency in the United States. *Proceedings of the National Academy of Sciences* **101:** 4136–4141.

McKee TB, Doesken NJ, Kleist NJ. 1993. The relationship of drought frequency and duration to time scales. Preprints, *Eighth Conf. on Applied Climatology*, Anaheim, CA, American Meteorological Society 179–184.

Meehl GA, Zwiers F, Evans J, Knutson T, Mearns L, Whetton P. 2000. Trends in extreme weather and climate events: Issues related to modeling extremes in projections of future climate change*. *Bull. Amer. Meteor. Soc*. **81(3):** 427–436.

R Development Core Team. 2012. R: A language and environment for statistical computing. R Foundation for Statistical Computing, Vienna, Austria. ISBN 3-900051-07-0. Available from: http://www.R-project.org.

Seager R, Kushnir Y, Ting M, Cane M, Naik N, Miller J. 2008. Would advance knowledge of 1930s SSTs have allowed prediction of the Dust Bowl drought? *J. Climate* **21:** 3261–

3281.

Schubert SD, and Coauthors. 2009. A U.S. CLIVAR project to assess and compare the responses of global climate models to drought-related SST forcing patterns: Overview and results. *J. Climate* **22:** 5251–5272.

Trenberth KE, Jones PD, Ambenje P, Bojariu R, Easterling D, Klein Tank A, Parker D, Rahimzadeh F, Renwick JA, Rusticucci M, Soden B, Zhai P. 2007. Observations: Surface and Atmospheric Climate Change. In *Climate Change 2007: The Physical Science Basis.* Contribution of Working Group I to the Fourth Assessment Report of the Intergovernmental Panel on Climate Change, Solomon S, Qin D, Manning M, Chen Z, Marquis M, Averyt KB, Tignor M. Miller HL (eds). Cambridge University Press: Cambridge, UK and New York, NY.

Yu M, Li Q, Hayes M.J, Svoboda MD, Heim RR. 2014. Are droughts becoming more frequent or severe in China based on the standardized precipitation evapotranspiration index: 1951–2010? *Int. J. Climatol*. **34:** 545–558.

Vicente-Serrano SM, Beguería S, López-Moreno JI. 2010. A multiscalar drought index sensitive to global warming: The Standardized Precipitation Evapotranspiration Index. *J. Climate* **23:** 1696–1718.

Wernli H, Paulat M, Hagen M, Frei C. 2008. SAL—A novel quality measure for the verification of quantitative precipitation forecasts. *Mon. Wea. Rev*. **136:** 4470–4487.

WMO. 2006. Drought monitoring and early warning: Concepts, progress and future

challenges. WMO.

Yager RR, Ovchinnikov S, Tong RM, Hguyen HT. 1987. Fuzzy sets and applications, Selected Papers by L. A. Zadeh. John Wiley and Sons.

Figure 1. Topography map of the upper Colorado River basin (UCRB). The outline of the map of the contiguous United States showing the location of UCRB is shown in the inset.

Figure 2. Time series of the number of drought objects for different combinations of parameter choices in MODE.

Figure 3. The spatial distributions of the values of (a) SPEI36, (b) SPI36, and clusters of drought objects identified for (c) SPEI36 and (d) SPI36 for 1960. The colored numbers in (c) and (d) indicate the objects that were matched between the two fields.

Figure 4. The statistics of (a) 10th, (b) 50th and (c) 90th percentile intensity attribute within drought objects for SPEI36 and SPI36 for 1950–2012.

Figure 5. Boxplot comparing the statistics of centroid (a) latitude and (b) longitude of drought objects between SPEI36 and SPI36 for 1950–2012.

Figure 6. The statistics of area of drought objects for SPEI36 and SPI36 for 1950–2012.

Figure 7. Relationship between SPEI36 and SPI36 median of the (a) 10th, (b) 50th, and (c) 90th percentile intensity attribute for merged cluster drought objects.

Figure 8. Relationship between SPEI36 and SPI36 median of centroid (a) latitude and (b) longitude attribute for merged cluster drought objects.

Figure 9. Relationship between SPEI36 and SPI36 (a) median and (b) mean of area of merged cluster drought objects.

Figure 10. The CSI for matched drought object area. The horizontal dash-dash line is the standard deviation, Ã

Figure 11. Bias in (a) area and (b) percentile intensity of matched cluster pairs of drought objects. The horizontal dash-dash line is the standard deviation, Ã

Figure A1. Normality plot of (a, b) 10th, (c, d) 50th, and (e, f) 90th percentile intensity of drought objects from (top) SPEI36 and (below) SPI36.

Figure A1. Normality plot of (a, b) latitude, (c, d) longitude, and (e, f) area of drought objects from (top) SPEI36 and (below) SPI36.

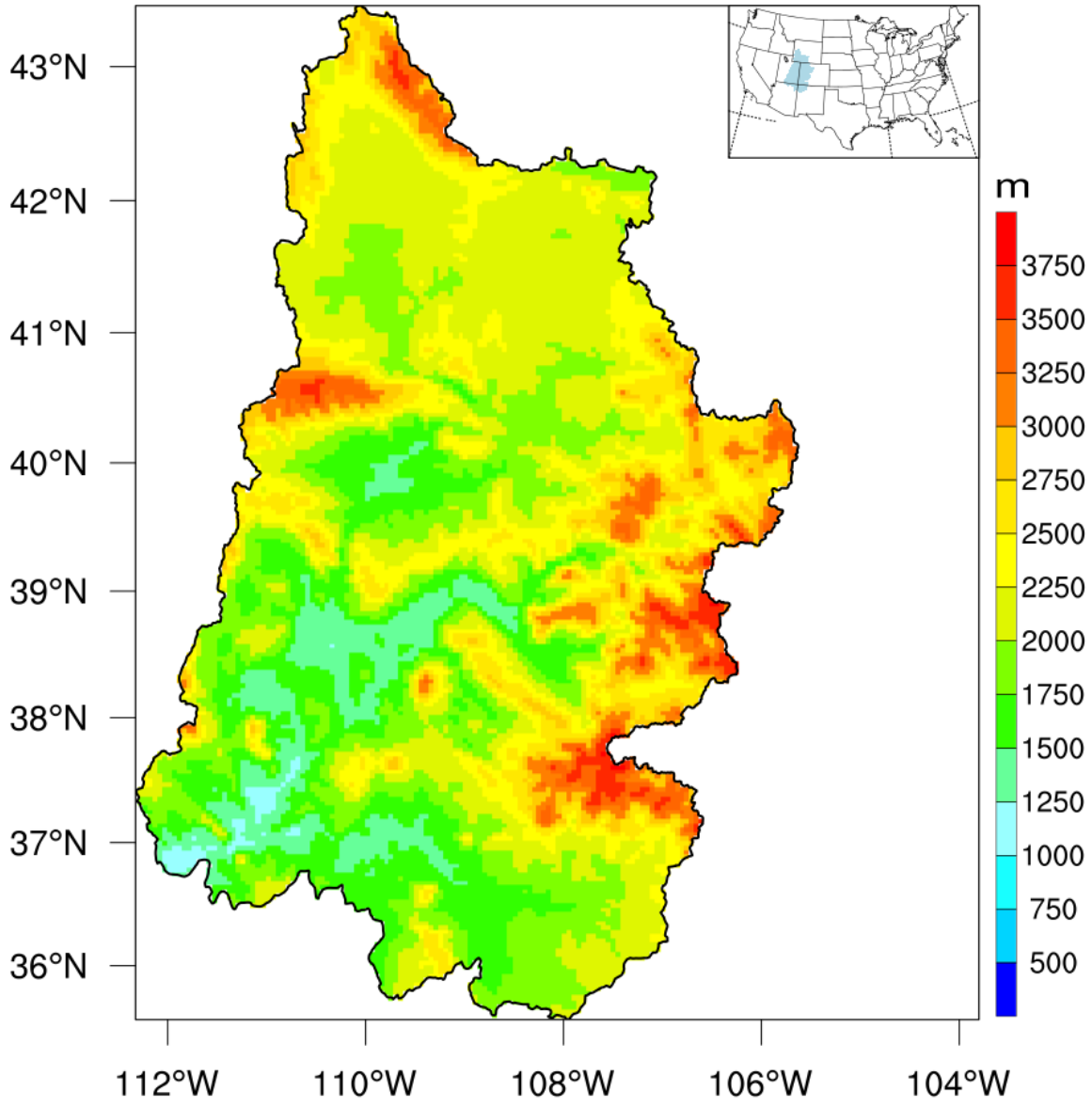

Figure 1. Topography map of the upper Colorado River basin (UCRB). The outline of the map of the contiguous United States showing the location of UCRB is shown in the inset.

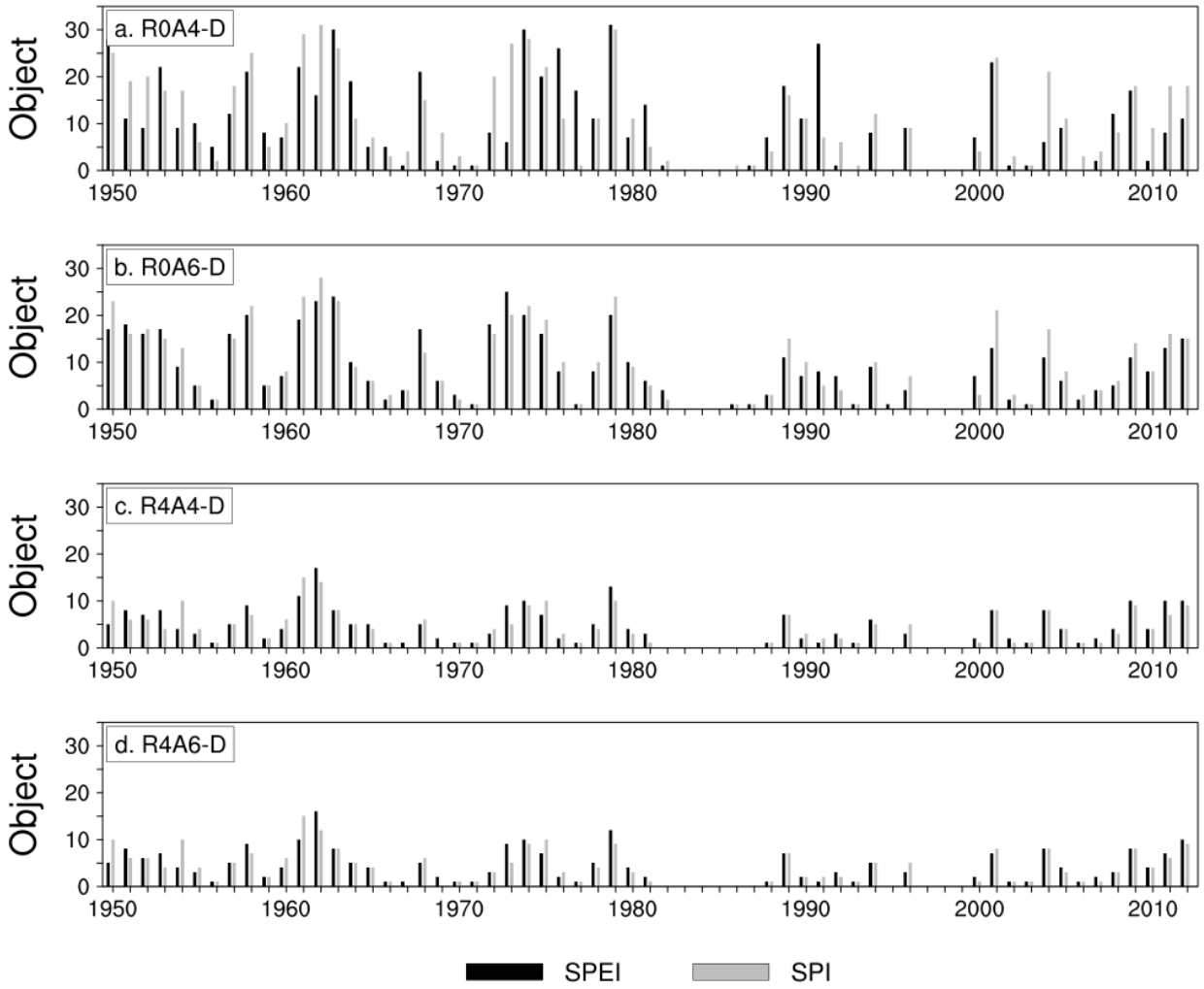

Figure 2. Time series of the number of drought objects for different combinations of parameter choices in MODE.

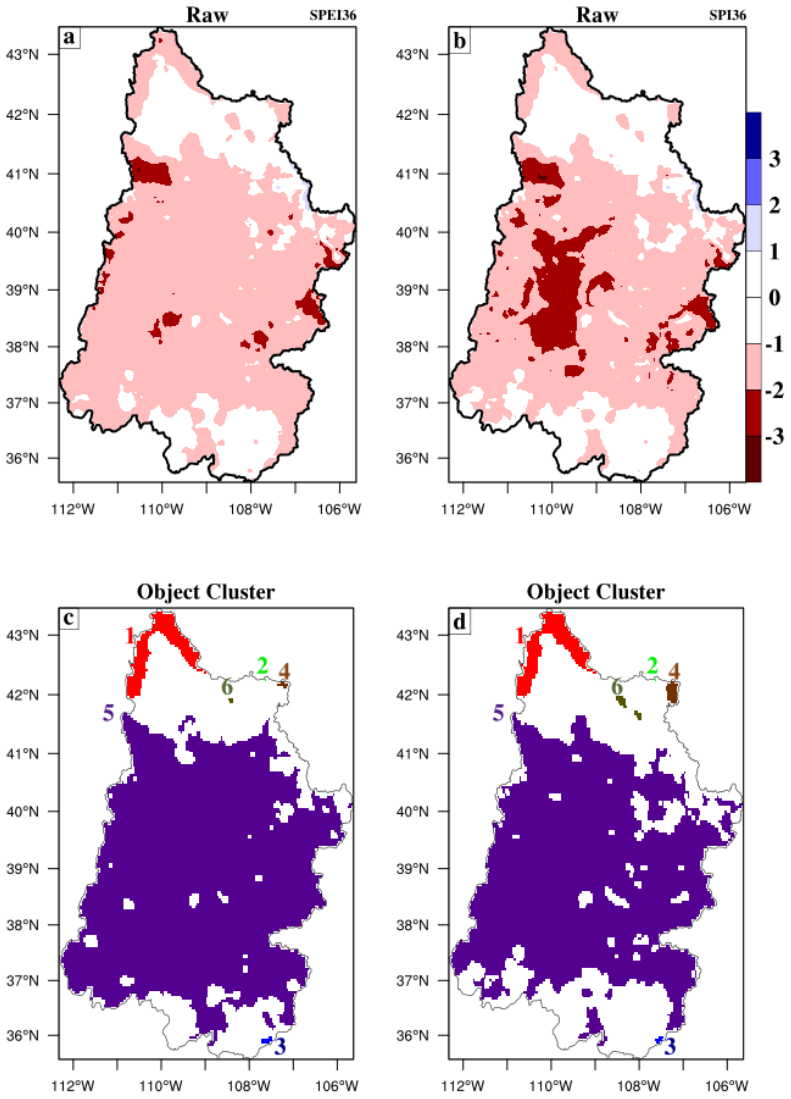

Figure 3. The spatial distributions of the values of (a) SPEI36, (b) SPI36, and clusters of drought objects identified for (c) SPEI36 and (d) SPI36 for 1960. The colored numbers in (c) and (d) indicate the objects that were matched between the two fields.

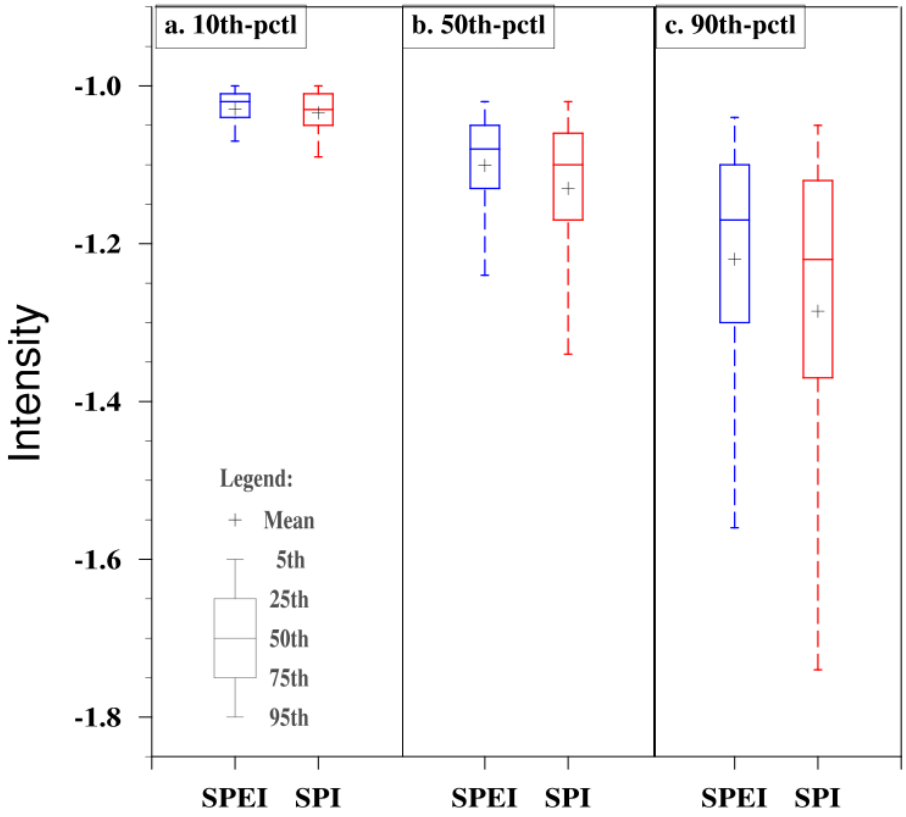

Figure 4. The statistics of (a) 10th, (b) 50th and (c) 90th percentile intensity attribute within drought objects for SPEI36 and SPI36 for 1950–2012.

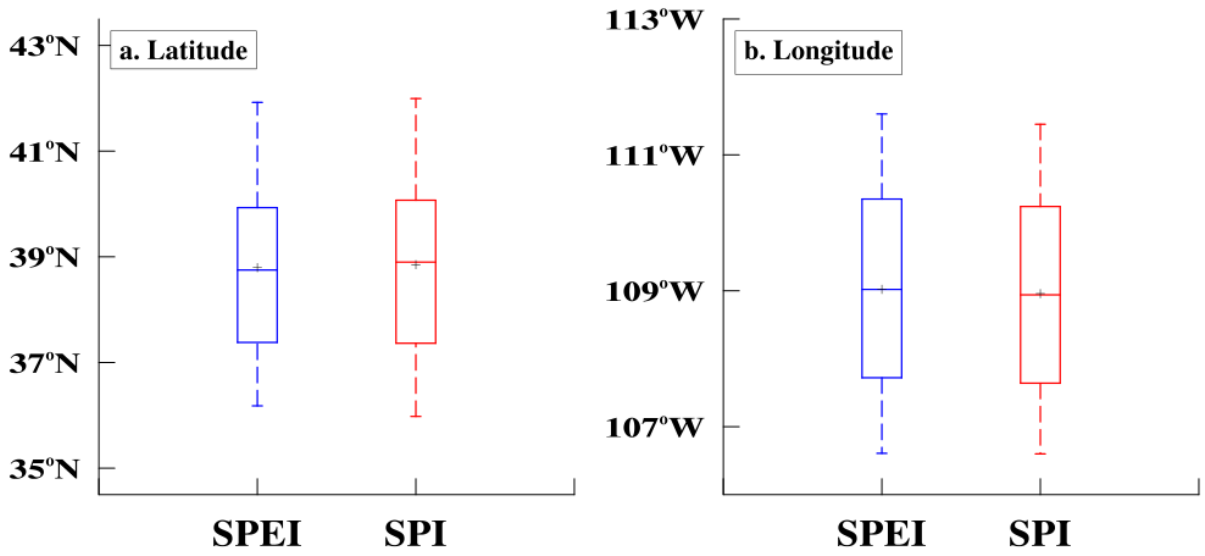

Figure 5. Boxplot comparing the statistics of centroid (a) latitude and (b) longitude of drought objects between SPEI36 and SPI36 for 1950–2012.

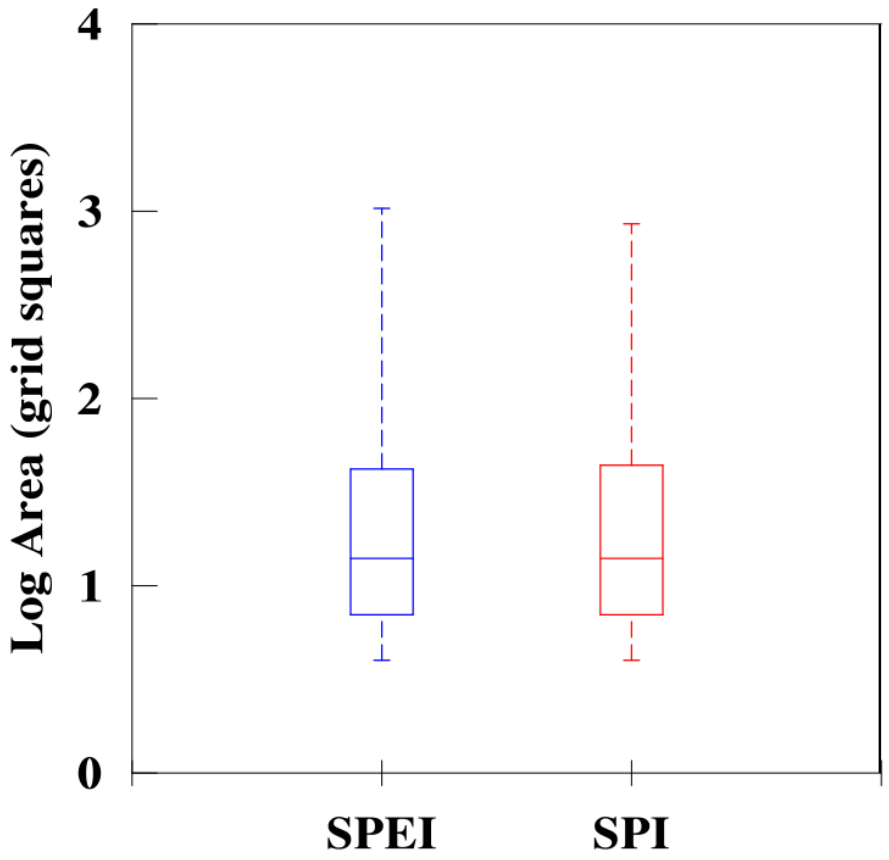

Figure 6. The statistics of area of drought objects for SPEI36 and SPI36 for 1950–2012.

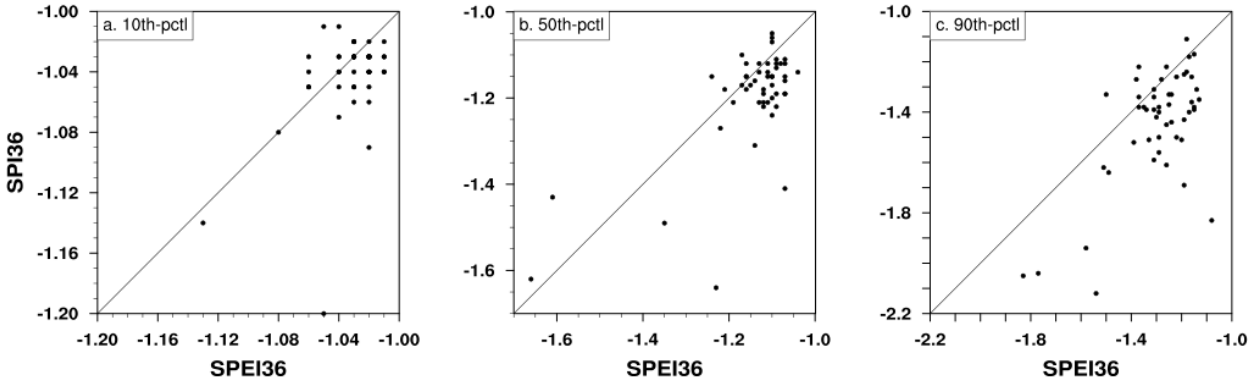

Figure 7. Relationship between SPEI36 and SPI36 median of the (a) 10th, (b) 50th, and (c) 90th percentile intensity attribute for merged cluster drought objects.

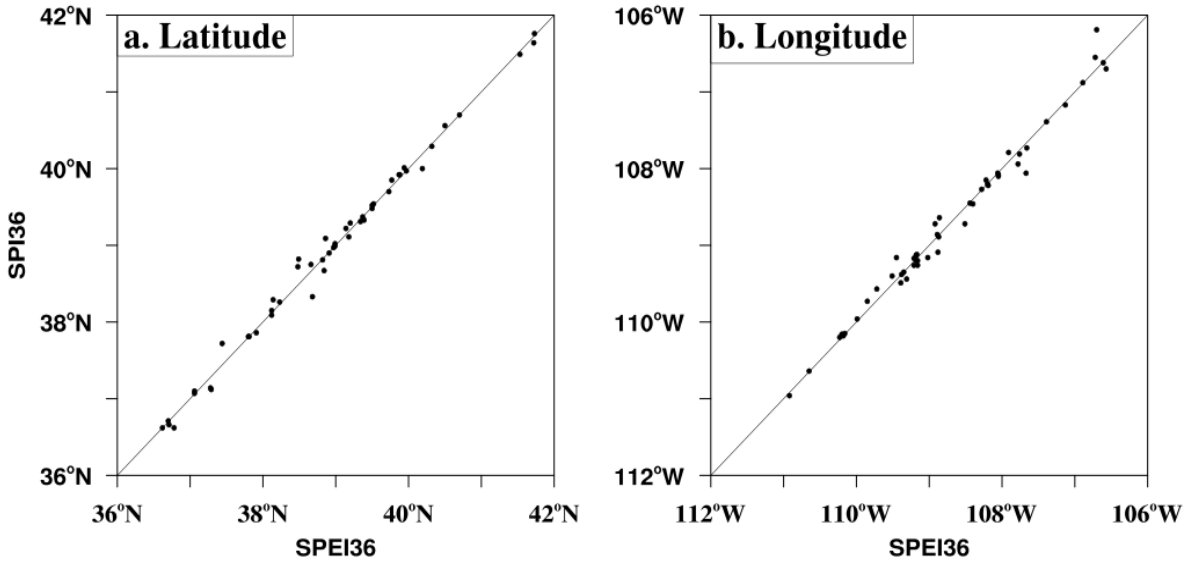

Figure 8. Relationship between SPEI36 and SPI36 median of centroid (a) latitude and (b) longitude attribute for merged cluster drought objects.

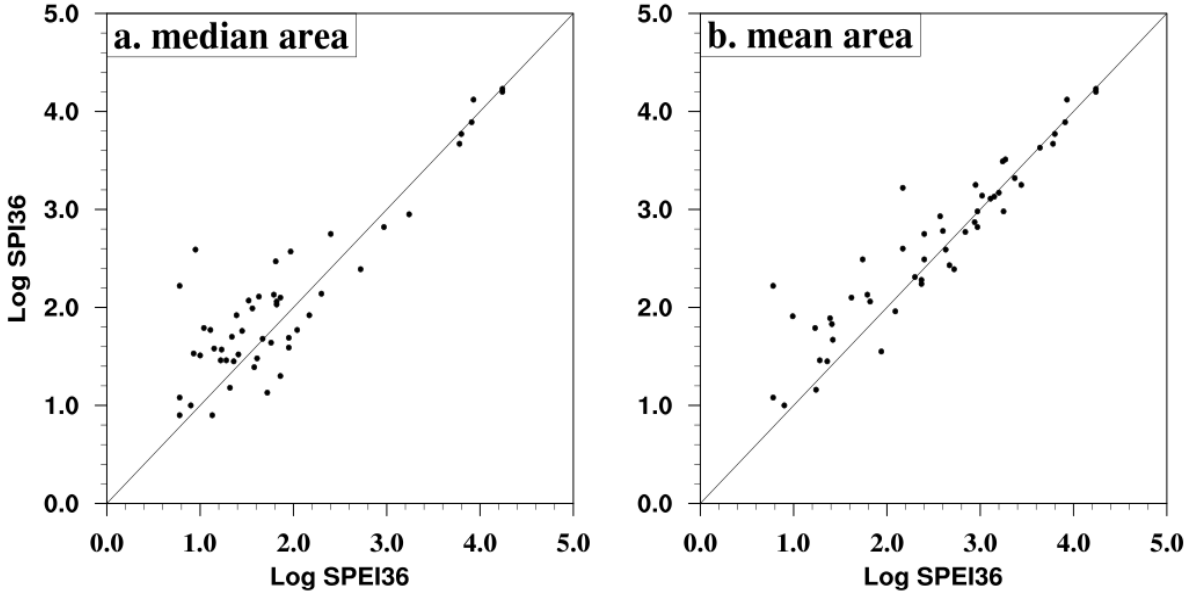

Figure 9. Relationship between SPEI36 and SPI36 (a) median and (b) mean of area of merged cluster drought objects.

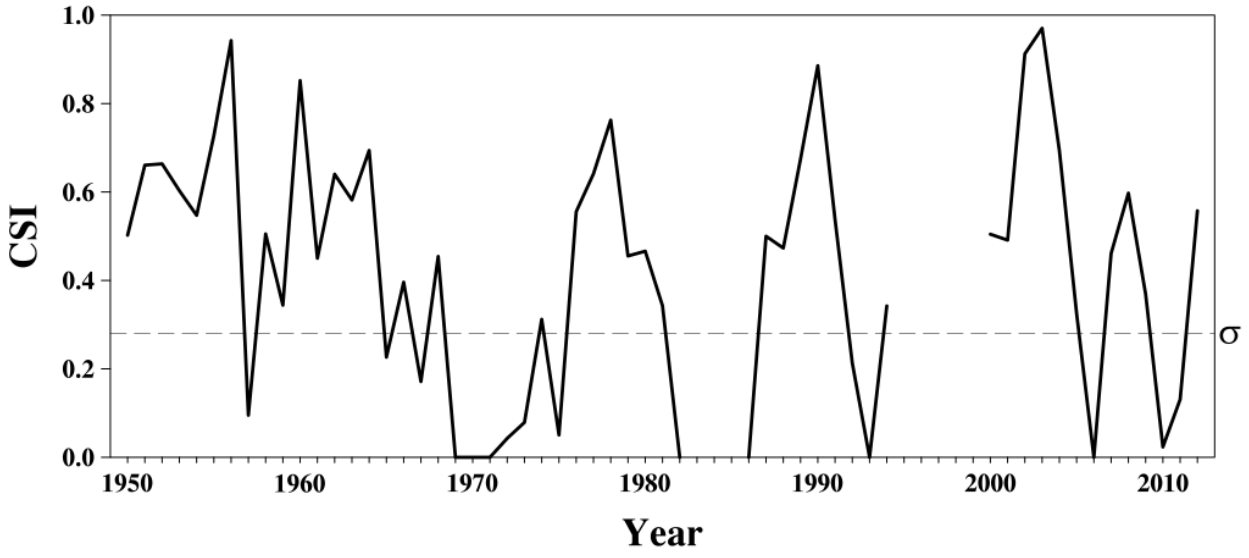

Figure 10. The CSI for matched drought object area. The horizontal dash-dash line is the standard deviation, Ã

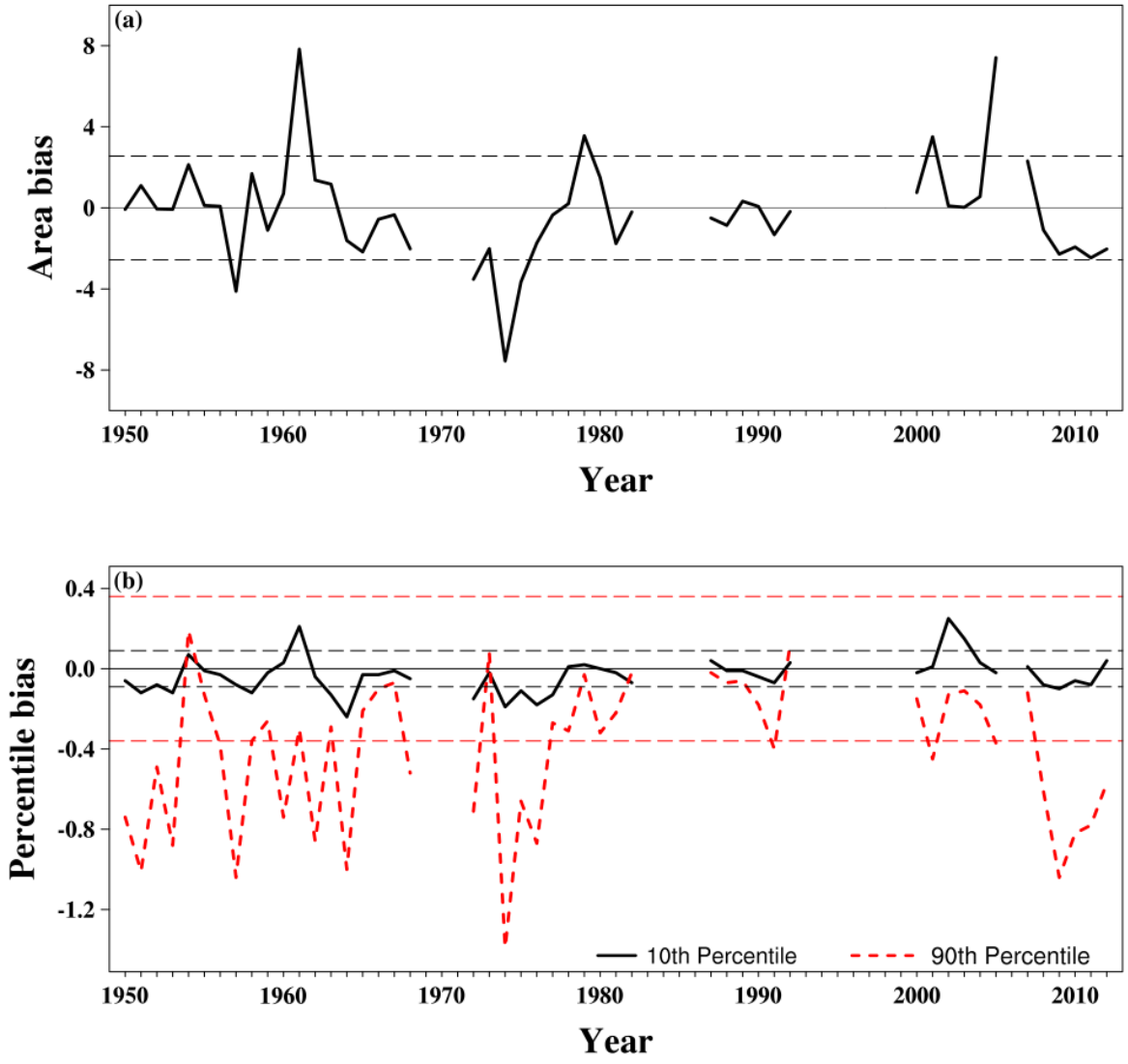

Figure 11. Bias in (a) area and (b) percentile intensity of matched cluster pairs of drought objects. The horizontal dash-dash line is the standard deviation, Ã

Appendix:

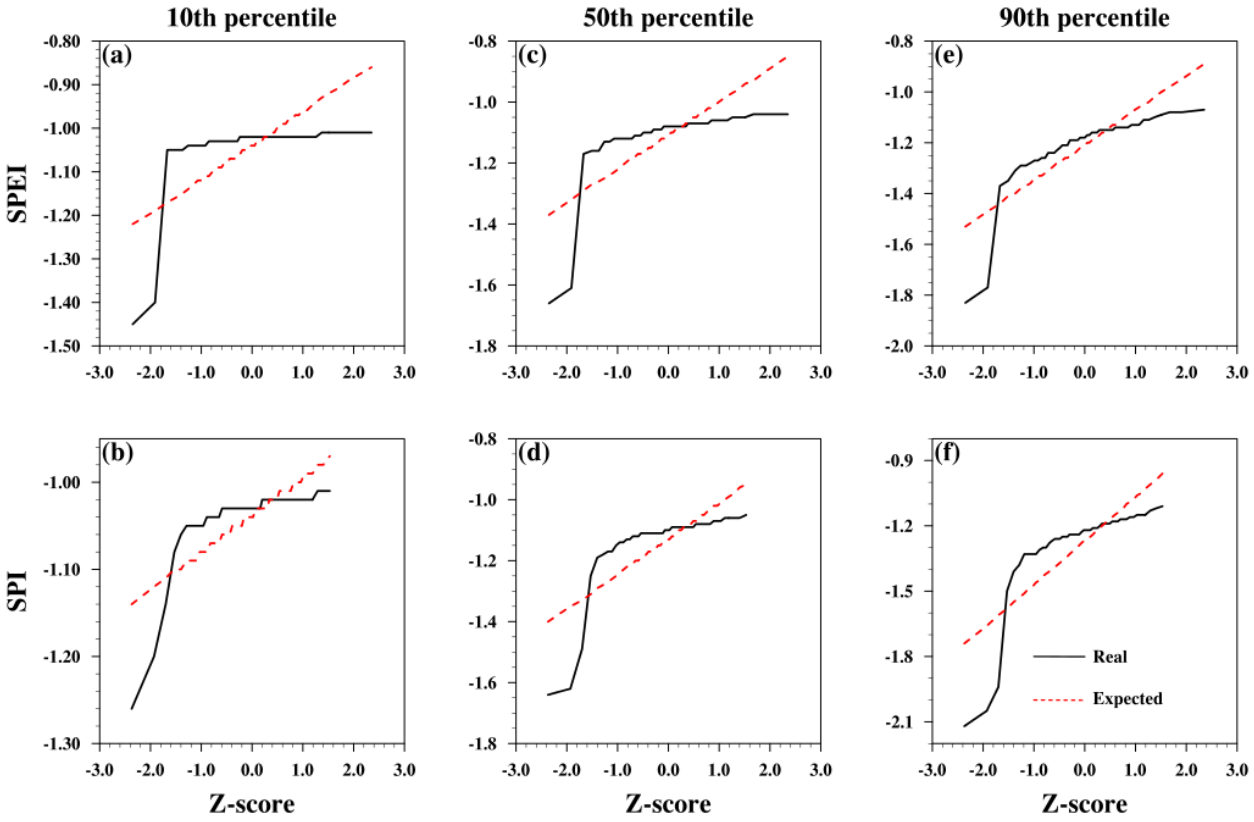

Figure A1. Normality plot of (a, b) 10th, (c, d) 50th, and (e, f) 90th percentile intensity of drought objects from (top) SPEI36 and (below) SPI36.

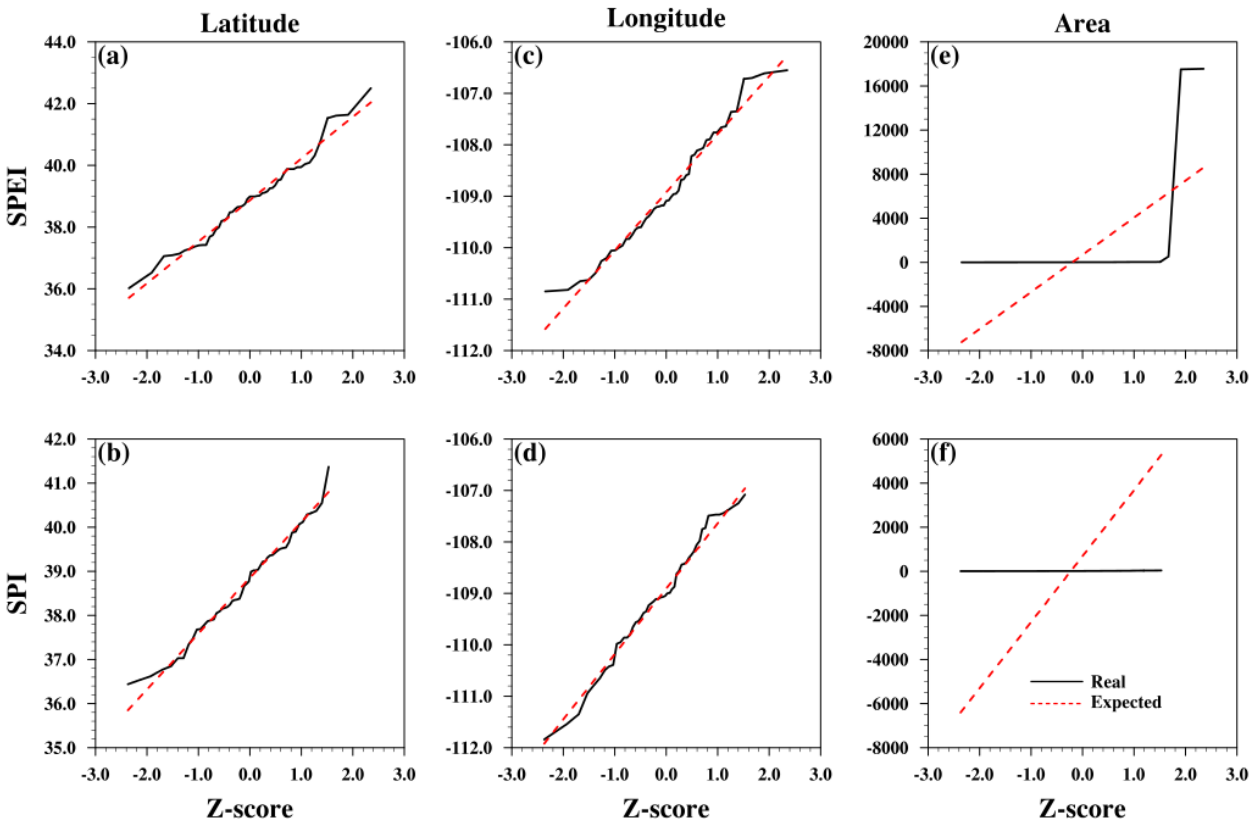

Figure A2. Normality plot of (a, b) latitude, (c, d) longitude, and (e, f) area of drought objects from (top) SPEI36 and (below) SPI36.

Statistics of Multi-year Droughts from the Method for Object-Based Diagnostic Evaluation (MODE)

Abayomi A. Abatan[1,*], William J. Gutowski, Jr., Caspar M. Ammann, Laurna Kaatz, Barbara G. Brown, Lawrence Buja, Randy Bullock, Tressa Fowler, Eric Gilleland and John Halley Gotway

- Examination and comparison of the statistics of drought attributes over the upper Colorado River basin using the Method for Object-based Diagnostic Evaluation (MODE) technique.
- Drought objects are based on the standardized precipitation index (SPI) and the standardized precipitation evapotranspiration index (SPEI) on a 36-month timescale (SPI36 and SPEI36, respectively).
- SPI36 produces more drought objects than SPEI36.
- SPI36 produces higher percentile intensity of drought objects than does SPEI36, which is clearly obvious in the 90th percentile intensity of drought objects.

[1]Corresponding author address: Abayomi A. Abatan, 3134 Agronomy Hall, Department of Geological and Atmospheric Sciences, Iowa State University, Ames, Iowa 50011 USA.

E-mail address: yomiabatan69@gmail.com

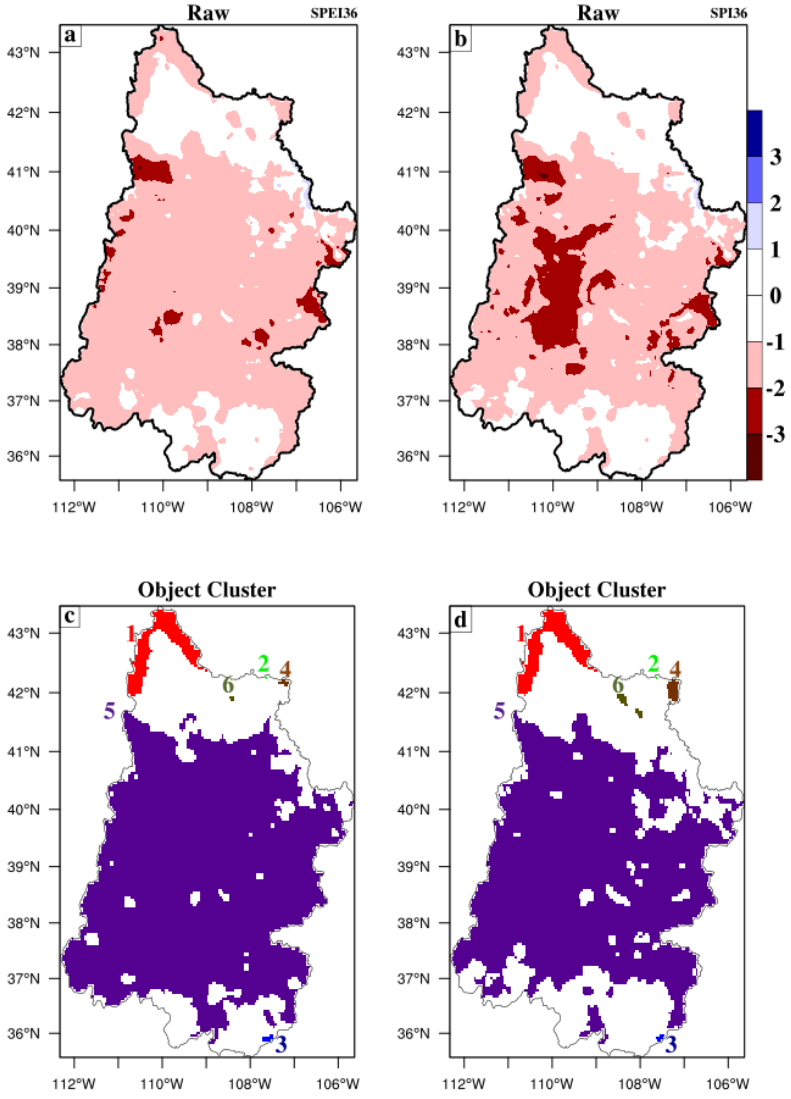

Table 1. Number of objects identified by drought indices relative to parameter threshold.

Table 2. The total interest matrix for each SPEI36–SPI36 simple drought object pair for December 1960.

Table 3. Attributes of merged cluster drought objects for December 1960.

Table 4. Approximate mean values for drought objects attributes from the drought indices

Table 1. Number of objects identified by drought indices relative to parameter threshold.

	Drought parameter			
Drought index	R0A4	R0A6	R4A4	R4A6
SPEI	617	534	260	249
SPI	680	573	244	241

Table 2. The total interest matrix for each SPEI36–SPI36 simple drought object pair for December 1960.

		SPEI36						
	Object	1	2	3	4	5	6	7
SPI36	1	**1.0000**			0.5188		0.5536	
	2		**1.0000**		0.5717			
	3		0.5393	**0.9228**			0.5350	
	4	0.5167		0.6545	**0.9189**	0.6153		
	5		0.5526	0.6802	**0.7046**			
	6		0.6664	0.5466			**0.8571**	
	7	0.5543				**0.8636**	**1.0000**	0.5817
	8						**0.8532**	0.5575
	9						**0.8315**	
	10						0.5785	**0.9697**

The bold values show total interest values greater than 0.7.

Table 3. Attributes of merged cluster drought objects for December 1960.

CLUS PAIR	SPEI36						SPI36					
	Intensity			Area	Location		Intensity			Area	Location	
	INT 10	INT 50	INT 90		Lat	Lon	INT 10	INT 50	INT 90		Lat	Lon
1	–1.12	–1.32	–1.56	505	42.4	–110.1	–1.08	–1.43	–1.77	528	42.4	–110.1
2	–1.09	–1.13	–1.18	6	42.0	–107.8	–1.03	–1.05	–1.09	5	42.0	–107.9
3	–1.01	–1.05	–1.24	30	35.8	–107.8	–1.04	–1.20	–1.61	19	35.9	–107.8
4	–1.04	–1.12	–1.38	26	41.8	–107.5	–1.06	–1.24	–1.49	63	41.8	–107.5
5	–1.15	–1.59	–1.96	13445	38.6	–109.2	–1.14	–1.58	–2.13	11891	38.7	–109.2
6	–1.01	–1.09	–1.16	12	41.6	–108.6	–1.04	–1.17	–1.57	51	41.5	–108.4
Sum	-6.42	-7.30	-8.47	14024	242.31	-651.08	-6.39	–7.66	-9.66	12557	242.23	-650.89
Mean	-1.07	-1.22	-1.41	2337.3	40.38	-108.51	-1.06	–1.28	-1.61	2092.8	40.37	-108.48
Median	**-1.06**	**-1.12**	**-1.31**	**28**	**41.72**	**-108.22**	**-1.05**	**–1.22**	**-1.59**	**57**	**41.64**	**-108.15**
Max	-1.15	-1.59	-1.96	6	42.41	-110.15	-1.14	–1.58	-2.13	5	42.41	-110.12
Min	-1.01	-1.05	-1.16	13445	35.85	-107.45	-1.03	–1.05	-1.09	11891	35.89	-107.49

Table 4. Approximate mean values for drought objects attributes from the drought indices

Drought Index	Attributes of drought objects					
	Percentile Intensity			Centroid location		
	10th	50th	90th	Latitude (°N)	Longitude (°W)	Log_{10} Area
SPI36	–1.038	–1.130	–1.270	38.9	108.9	1.32
SPEI36	–1.040	–1.110	–1.210	38.9	108.9	1.28